

UC Davis

UC Davis Previously Published Works

Title

C 1 and C 2 interpolation of orientation data along spatial Pythagorean-hodograph curves using rational adapted spline frames

Permalink

<https://escholarship.org/uc/item/72p18517>

Authors

Moon, Hwan Pyo
Farouki, Rida T

Publication Date

2018-11-01

DOI

10.1016/j.cagd.2018.07.005

Peer reviewed

C^1 and C^2 interpolation of orientation data along spatial Pythagorean-hodograph curves using rational adapted spline frames

Hwan Pyo Moon
Department of Mathematics,
Dongguk University–Seoul, Seoul 04620, Republic of Korea.

Rida T. Farouki
Department of Mechanical and Aerospace Engineering,
University of California, Davis, CA 95616, USA.

Abstract

The problem of constructing a rational adapted frame $(\mathbf{f}_1(\xi), \mathbf{f}_2(\xi), \mathbf{f}_3(\xi))$ that interpolates a discrete set of orientations at specified nodes along a given spatial Pythagorean–hodograph (PH) curve $\mathbf{r}(\xi)$ is addressed. PH curves are the only polynomial space curves that admit rational adapted frames, and the Euler–Rodrigues frame (ERF) is a fundamental instance of such frames. The ERF can be transformed into other rational adapted frame by applying a rationally–parametrized rotation to the normal–plane vectors. When orientation and angular velocity data at curve end points are given, a Hermite frame interpolant can be constructed using a complex quadratic polynomial that parametrizes the normal–plane rotation, by an extension of the method recently introduced to construct a rational minimal twist frame (MTF). To construct a rational adapted spline frame, a representation that resolves potential ambiguities in the orientation data is introduced. Based on this representation, a C^1 rational adapted spline frame is constructed through local Hermite interpolation on each segment, using angular velocities estimated from a cubic spline that interpolates the frame phase angle relative to the ERF. To construct a C^2 rational adapted spline frame, which ensures continuity of the angular acceleration, a complex–valued cubic spline is used to directly interpolate the complex exponentials of the phase angles at the nodal points.

Keywords: rational adapted spline frames, twist, angular velocity, angular acceleration, Pythagorean–hodograph curves, rotation–minimizing frame, Euler–Rodrigues frame.

e–mail addresses: hpmoon@dongguk.edu, farouki@ucdavis.edu

1 Introduction

The spatial motion of a rigid body is defined by specifying its position and orientation at each instant. The position may be specified as a parametric curve $\mathbf{r}(\xi)$ describing the path of a distinguished point (such as the center of mass), and the orientation may be specified by an orthonormal frame $(\mathbf{f}_1(\xi), \mathbf{f}_2(\xi), \mathbf{f}_3(\xi))$ defined along $\mathbf{r}(\xi)$. In many applications, an *adapted* frame that satisfies $\mathbf{f}_1(\xi) = \mathbf{r}'(\xi)/|\mathbf{r}'(\xi)|$ — i.e., the first frame vector coincides with the tangent to the path $\mathbf{r}(\xi)$ — is desired, so that $\mathbf{f}_2(\xi)$ and $\mathbf{f}_3(\xi)$ span the curve normal plane. Clearly, there are infinitely many adapted frames, corresponding to different choices for the variation of the orientation of $\mathbf{f}_2(\xi)$ and $\mathbf{f}_3(\xi)$ along $\mathbf{r}(\xi)$.

The *rotation minimizing frame* (RMF) or *Bishop frame* [1] is an important type of adapted frame $(\mathbf{t}, \mathbf{u}, \mathbf{v})$ on a space curve, consisting of the curve tangent \mathbf{t} and unit normal-plane vectors \mathbf{u} and \mathbf{v} that exhibit no instantaneous rotation about \mathbf{t} — i.e., the tangent component of the frame angular velocity vanishes. Since polynomial/rational curves do not ordinarily admit rational RMFs, many schemes to approximate them have been proposed [8, 15, 16, 18, 19, 20, 23, 24, 25, 26]. On the other hand, the identification of space curves that admit exact rational RMFs has recently become a topic of active investigation [4, 6, 11, 12]. Such curves are necessarily a subset of the Pythagorean-hodograph (PH) curves [3], since only PH curves possess rational unit tangents. The Frenet frames of PH curves have also been studied for cubic helical spline curves [13].

The focus of the present study is the construction of rational adapted spline frames along a pre-defined spatial PH curve, that interpolate prescribed frame orientations at a sequence of specified curve points with C^1 or C^2 continuity — where C^1 implies continuity of angular velocity, and C^2 implies continuity of angular velocity *and* angular acceleration. Smoothness of orientational motion is as important as that of translational motion in applications, since discontinuity of angular velocity and acceleration is physically impossible in the steering of devices such robot end effectors, unmanned aerial vehicles, or spacecraft.

Algorithms to construct rigid body motions specified by rational adapted RMFs with given initial/final positions and orientations have recently been developed [7, 9]. However, since the computation of an RMF is an initial value problem, the path $\mathbf{r}(\xi)$ is an outcome of these algorithms, rather than being specified *a priori*. Interpolation algorithms to construct rigid body motions for general orientations, without imposing the adaptedness condition, have been proposed [14, 17, 21]. These algorithms also compute the rotations and the trajectories simultaneously. In the present study, we consider adapted motions along a prescribed spatial PH curve $\mathbf{r}(\xi)$ that matches a sequence of specified orientations at nodal points along it, with continuity of angular velocity and acceleration at those points. In this context, the rotation-minimizing condition is relaxed, since an RMF cannot (in general) match given orientations at distinct points along pre-defined curve.

The *Euler-Rodrigues frame* (ERF) is a rational adapted frame defined on any spatial Pythagorean-hodograph curve [2]. The ERF serves as a starting point for the construction of other rational adapted frames, by applying a rationally-

parametrized rotation to the two ERF normal plane vectors. Such rotations are defined by a pair of real polynomials, or equivalently a single complex-valued polynomial, whose coefficients can be used to make the new frame satisfy given constraints on its orientation, angular velocity, and angular acceleration.

This method has been used [10] to construct a rational *minimal twist frame* (MTF) along a given curve, i.e., an adapted frame that satisfies prescribed initial/final orientations without any unnecessary twist between them. As a special type of MTF, one may consider frames with a constant angular velocity. However, such frames do not admit a rational parameterization, even for PH curves. A rational MTF can be constructed by controlling the angular velocity using a rational rotation of the ERF.

This capability is exploited in the present study to construct rational spline frames on pre-defined PH curves with given orientations at a sequence of nodal points, and C^1 or C^2 continuity of the frame orientation at those points. The method is based on defining a complex-valued piecewise-polynomial function that specifies the frame rotation relative the ERF. For a C^1 spline frame, a local Hermite interpolation scheme between successive nodes is developed by estimating nodal angular velocities from the given orientation data. To achieve C^2 continuity, more degrees of freedom are needed, and we employ a complex-valued cubic spline function to define the frame rotation relative to the ERF.

The remainder of this paper is organized as follows. Section 2 reviews some basic properties of PH curves, and various rational adapted frames defined on them — including the Euler–Rodrigues frame, rotation–minimizing frame, and minimal–twist frame. A Hermite interpolation scheme for a rational adapted frame with prescribed initial/final orientations and angular velocities is then developed in Section 3. This scheme is then generalized in Section 4 to develop algorithms for rational adapted spline frames that match a sequence of specified orientations at given curve points with C^1 or C^2 continuity, and a number of computed examples are presented to illustrate the results of these algorithms. Finally, Section 5 summarizes the key results of the present study.

2 Rational adapted frames on PH curves

The variation of a right-handed orthonormal frame $(\mathbf{f}_1(\xi), \mathbf{f}_2(\xi), \mathbf{f}_3(\xi))$ along a space curve $\mathbf{r}(\xi)$ is characterized by its *angular velocity* $\boldsymbol{\omega}$ through the relations

$$\frac{d\mathbf{f}_1}{ds} = \dot{\mathbf{f}}_1 = \boldsymbol{\omega} \times \mathbf{f}_1, \quad \frac{d\mathbf{f}_2}{ds} = \dot{\mathbf{f}}_2 = \boldsymbol{\omega} \times \mathbf{f}_2, \quad \frac{d\mathbf{f}_3}{ds} = \dot{\mathbf{f}}_3 = \boldsymbol{\omega} \times \mathbf{f}_3,$$

where dots denote derivatives¹ with respect to arc length s . The angular velocity $\boldsymbol{\omega}$ can be expressed in terms of the frame $(\mathbf{f}_1, \mathbf{f}_2, \mathbf{f}_3)$ itself as

$$\boldsymbol{\omega} = \omega_1 \mathbf{f}_1 + \omega_2 \mathbf{f}_2 + \omega_3 \mathbf{f}_3, \tag{1}$$

¹Throughout this paper, dots indicate derivatives with respect to arc length s , and primes indicate derivatives with respect to a general curve parameter ξ .

with components defined by

$$\omega_1 = \dot{\mathbf{f}}_2 \cdot \mathbf{f}_3 = -\dot{\mathbf{f}}_3 \cdot \mathbf{f}_2, \quad \omega_2 = \dot{\mathbf{f}}_3 \cdot \mathbf{f}_1 = -\dot{\mathbf{f}}_1 \cdot \mathbf{f}_3, \quad \omega_3 = \dot{\mathbf{f}}_1 \cdot \mathbf{f}_2 = -\dot{\mathbf{f}}_2 \cdot \mathbf{f}_1.$$

A spatial PH curve $\mathbf{r}(\xi)$ may be generated [3] from a quaternion polynomial

$$\mathcal{A}(\xi) = u(\xi) + v(\xi) \mathbf{i} + p(\xi) \mathbf{j} + q(\xi) \mathbf{k} \quad (2)$$

by integrating the hodograph

$$\begin{aligned} \mathbf{r}'(\xi) = \mathcal{A}(\xi) \mathbf{i} \mathcal{A}^*(\xi) &= [u^2(\xi) + v^2(\xi) - p^2(\xi) - q^2(\xi)] \mathbf{i} \\ &+ 2[u(\xi)q(\xi) + v(\xi)p(\xi)] \mathbf{j} + 2[v(\xi)q(\xi) - u(\xi)p(\xi)] \mathbf{k}, \end{aligned}$$

where $\mathcal{A}^*(\xi) = u(\xi) - v(\xi) \mathbf{i} - p(\xi) \mathbf{j} - q(\xi) \mathbf{k}$ is the conjugate of $\mathcal{A}(\xi)$. This curve has the polynomial parametric speed

$$\sigma(\xi) = |\mathbf{r}'(\xi)| = |\mathcal{A}(\xi)|^2 = u^2(\xi) + v^2(\xi) + p^2(\xi) + q^2(\xi). \quad (3)$$

Any spatial PH curve admits an adapted frame $(\mathbf{e}_1, \mathbf{e}_2, \mathbf{e}_3)$ known [2] as the *Euler–Rodrigues frame* (ERF), defined by the expressions

$$\mathbf{e}_1(\xi) := \frac{\mathcal{A}(\xi) \mathbf{i} \mathcal{A}^*(\xi)}{|\mathcal{A}(\xi)|^2}, \quad \mathbf{e}_2(\xi) := \frac{\mathcal{A}(\xi) \mathbf{j} \mathcal{A}^*(\xi)}{|\mathcal{A}(\xi)|^2}, \quad \mathbf{e}_3(\xi) := \frac{\mathcal{A}(\xi) \mathbf{k} \mathcal{A}^*(\xi)}{|\mathcal{A}(\xi)|^2}.$$

Since the denominator in these expressions is the polynomial parametric speed (3), the ERF is a *rational* frame in which \mathbf{e}_1 is the curve tangent while $\mathbf{e}_2, \mathbf{e}_3$ span the normal plane. The ERF angular velocity may be expressed as

$$\boldsymbol{\omega} = \omega_1 \mathbf{e}_1 + \omega_2 \mathbf{e}_2 + \omega_3 \mathbf{e}_3, \quad (4)$$

with components defined [5] by

$$\begin{aligned} \omega_1 = \dot{\mathbf{e}}_2 \cdot \mathbf{e}_3 = -\dot{\mathbf{e}}_3 \cdot \mathbf{e}_2 &= 2 \frac{uv' - u'v - pq' + p'q}{\sigma^2}, \\ \omega_2 = \dot{\mathbf{e}}_3 \cdot \mathbf{e}_1 = -\dot{\mathbf{e}}_1 \cdot \mathbf{e}_3 &= 2 \frac{up' - u'p + vq' - v'q}{\sigma^2}, \\ \omega_3 = \dot{\mathbf{e}}_1 \cdot \mathbf{e}_2 = -\dot{\mathbf{e}}_2 \cdot \mathbf{e}_1 &= 2 \frac{uq' - u'q - vp' + v'p}{\sigma^2}. \end{aligned}$$

The ERF $(\mathbf{e}_1, \mathbf{e}_2, \mathbf{e}_3)$ can be used to generate other rational adapted frames $(\mathbf{f}_1, \mathbf{f}_2, \mathbf{f}_3)$ by taking $\mathbf{f}_1 = \mathbf{e}_1$ and specifying $\mathbf{f}_2, \mathbf{f}_3$ through a rational normal–plane rotation of $\mathbf{e}_2, \mathbf{e}_3$ of the form

$$\begin{bmatrix} \mathbf{f}_2(\xi) \\ \mathbf{f}_3(\xi) \end{bmatrix} = \frac{1}{a^2(\xi) + b^2(\xi)} \begin{bmatrix} a^2(\xi) - b^2(\xi) & -2a(\xi)b(\xi) \\ 2a(\xi)b(\xi) & a^2(\xi) - b^2(\xi) \end{bmatrix} \begin{bmatrix} \mathbf{e}_2(\xi) \\ \mathbf{e}_3(\xi) \end{bmatrix}, \quad (5)$$

for relatively prime polynomials $a(\xi), b(\xi)$. This amounts to obtaining $\mathbf{f}_2, \mathbf{f}_3$ from $\mathbf{e}_2, \mathbf{e}_3$ by a normal–plane rotation through the *phase angle* defined by

$$\theta(\xi) := 2 \tan^{-1} \frac{b(\xi)}{a(\xi)}, \quad (6)$$

such that

$$\cos \theta(\xi) = \frac{a^2(\xi) - b^2(\xi)}{a^2(\xi) + b^2(\xi)}, \quad \sin \theta(\xi) = \frac{2a(\xi)b(\xi)}{a^2(\xi) + b^2(\xi)}.$$

The variation of the rational frame $(\mathbf{f}_1, \mathbf{f}_2, \mathbf{f}_3)$ consists of the variation of the ERF $(\mathbf{e}_1, \mathbf{e}_2, \mathbf{e}_3)$ and the variation of the rotation angle $\theta(\xi)$.

If $\boldsymbol{\Omega}$ is the angular velocity vector of the frame $(\mathbf{f}_1, \mathbf{f}_2, \mathbf{f}_3)$ expressed in terms of the ERF $(\mathbf{e}_1, \mathbf{e}_2, \mathbf{e}_3)$ as

$$\boldsymbol{\Omega} = \Omega_1 \mathbf{e}_1 + \Omega_2 \mathbf{e}_2 + \Omega_3 \mathbf{e}_3,$$

its components are

$$\Omega_1 = \omega_1 + \dot{\theta}, \quad \Omega_2 = \omega_2, \quad \Omega_3 = \omega_3 \quad (7)$$

where

$$\dot{\theta} = \frac{\theta'}{\sigma} = 2 \frac{ab' - a'b}{\sigma(a^2 + b^2)}. \quad (8)$$

The *rotation-minimizing frame* (RMF) is an important adapted frame $(\mathbf{t}, \mathbf{u}, \mathbf{v})$ consisting of the curve tangent \mathbf{t} and normal-plane vectors \mathbf{u}, \mathbf{v} that exhibit no rotation about \mathbf{t} — i.e., the angular velocity component ω_1 in (1) vanishes identically, so that $\boldsymbol{\omega}$ for RMF has the form

$$\boldsymbol{\omega} = \omega_2 \mathbf{u} + \omega_3 \mathbf{v}.$$

The identification of spatial PH curves that admit *rational* RMFs is equivalent to identifying conditions for the existence of polynomials $a(\xi), b(\xi)$ such that $\omega_1(\xi) + \theta'(\xi)/\sigma(\xi) \equiv 0$. This condition has been thoroughly analyzed in previous studies [4, 6, 11, 12] and it transpires that the lowest-order non-trivial solutions form a subset of the spatial PH quintics. In the present context, we emphasize that the construction of RMFs is an *initial value problem* — for a given space curve $\mathbf{r}(\xi), \xi \in [0, 1]$ it is impossible to prescribe both initial *and* final instances $\mathbf{t}(0), \mathbf{u}(0), \mathbf{v}(0)$ and $\mathbf{t}(1), \mathbf{u}(1), \mathbf{v}(1)$ of an RMF. Motivated by this observation, the notion of a *minimal twist frame* (MTF) was recently introduced in [10].

An MTF is an adapted orthonormal frame $\mathbf{f}_1(\xi), \mathbf{f}_2(\xi), \mathbf{f}_3(\xi)$ defined along a given space curve $\mathbf{r}(\xi), \xi \in [0, 1]$ matching prescribed initial and final instances $(\mathbf{f}_1(0), \mathbf{f}_2(0), \mathbf{f}_3(0))$ and $(\mathbf{f}_1(1), \mathbf{f}_2(1), \mathbf{f}_3(1))$ with the minimum amount of rotation of the normal plane vectors $\mathbf{f}_2(\xi), \mathbf{f}_3(\xi)$ about the tangent $\mathbf{f}_1(\xi)$ consistent with these boundary conditions. If $\boldsymbol{\Omega} = \Omega_1 \mathbf{f}_1 + \Omega_2 \mathbf{f}_2 + \Omega_3 \mathbf{f}_3$ is the angular velocity of an adapted frame $(\mathbf{f}_1, \mathbf{f}_2, \mathbf{f}_3)$ with prescribed initial/final instances, the minimal twist property is characterized by two conditions: (i) Ω_1 does not change sign on $\xi \in (0, 1)$, and (ii) it achieves the least possible absolute value for the *twist* integral, defined by

$$T := \int_0^S \Omega_1 ds = \int_0^1 \Omega_1(\xi) \sigma(\xi) d\xi,$$

where S is the total arc length of $\mathbf{r}(\xi)$. When the initial/final orientations of the frame are specified, the twist value should be the difference in the orientation of the frame normal–plane vectors, relative to RMF normal–plane vectors, between the final and initial instances. Thus, all possible values for the twist are equal to the minimal twist plus an integer multiple of 2π . Hence, condition (ii) specifies the frame twist value, while condition (i) avoids cancellation of clockwise and anti–clockwise rotation in the normal plane.

An ideal instance is the constant angular velocity MTF, characterized by the condition

$$\Omega_1(\xi) \equiv \bar{\Omega}_1 := \frac{T_{\min}}{S},$$

where T_{\min} is the least possible twist for prescribed end frames on a given curve. Although the constant angular velocity MTF admits a closed–form expression, it incurs transcendental functions. As an alternative, a rational MTF satisfying the constraints $\Omega_1(0) = \Omega_1(1) = \bar{\Omega}_1$ was proposed in [10] — this frame can be constructed from the ERF by applying the rational rotation (5) with quadratic polynomials $a(\xi)$ and $b(\xi)$, and furnishes one free parameter that can be used to minimize the mean square deviation of $\Omega_1(\xi)$ from $\bar{\Omega}_1$.

3 Hermite interpolation for rational frames

The problem of Hermite interpolation for rational adapted frames defined on a spatial PH curve consists of specifying initial/final orientations of the normal–plane vectors, and derivatives of their orientation. In an earlier study [10], we developed an algorithm to construct a rational MTF by solving a Hermite interpolation problem with given initial/final frame orientations and angular velocity data, assigned to be the mean angular velocity. We apply here a similar method to construct Hermite interpolants for general prescribed angular velocities. For convenience, we recall a few important notations and equations from [10].

Let $\mathbf{r}(\xi)$ be a spatial PH curve with ERF $(\mathbf{e}_1(\xi), \mathbf{e}_2(\xi), \mathbf{e}_3(\xi))$. The goal is to construct a rational adapted frame $(\mathbf{f}_1(\xi), \mathbf{f}_2(\xi), \mathbf{f}_3(\xi))$ of the form (5) on $\mathbf{r}(\xi)$ that satisfies C^1 boundary constraints, i.e., prescribed initial/final orientations and angular velocities. Combining the real polynomials $a(\xi)$, $b(\xi)$ into a complex polynomial $\mathbf{w}(\xi) = a(\xi) + i b(\xi)$, the angular function (6) satisfies

$$\exp(i\theta(\xi)) = \frac{\mathbf{w}^2(\xi)}{|\mathbf{w}(\xi)|^2} = \frac{\mathbf{w}(\xi)}{\bar{\mathbf{w}}(\xi)},$$

and its derivative can be expressed as

$$\theta'(\xi) = 2 \frac{\text{Im}(\bar{\mathbf{w}}(\xi)\mathbf{w}'(\xi))}{|\mathbf{w}(\xi)|^2} = 2 \text{Im}(\mathbf{w}'(\xi)/\mathbf{w}(\xi)).$$

Let the initial and final frame instances be specified as

$$(\mathbf{f}_1(0), \mathbf{f}_2(0), \mathbf{f}_3(0)) \quad \text{and} \quad (\mathbf{f}_1(1), \mathbf{f}_2(1), \mathbf{f}_3(1)), \quad (9)$$

where $\mathbf{f}_1(0)$ and $\mathbf{f}_1(1)$ coincide with the initial and final tangents of $\mathbf{r}(\xi)$, and the orientations of $\mathbf{f}_2(0), \mathbf{f}_3(0)$ and $\mathbf{f}_2(1), \mathbf{f}_3(1)$ relative to the ERF vectors $\mathbf{e}_2(0), \mathbf{e}_3(0)$ and $\mathbf{e}_2(1), \mathbf{e}_3(1)$ are defined by given initial/final values $\theta(0), \theta(1) \in (-\pi, \pi]$ of the angle function (6) through equation (5). Similarly, the end-point tangential components of the frame angular velocity $\Omega_1(\xi)$ are assigned given values

$$\Omega_1(0) \quad \text{and} \quad \Omega_1(1). \quad (10)$$

As noted in [10] a quadratic polynomial, expressed in Bernstein form as

$$\mathbf{w}(\xi) = \mathbf{w}_0 (1 - \xi)^2 + \mathbf{w}_1 2(1 - \xi)\xi + \mathbf{w}_2 \xi^2,$$

provides the minimum necessary flexibility to achieve a frame $(\mathbf{f}_1(\xi), \mathbf{f}_2(\xi), \mathbf{f}_3(\xi))$ satisfying the C^1 boundary conditions. Furthermore, since the angular function (6) remains unchanged on multiplying $\mathbf{w}(\xi)$ by any non-zero complex constant, we may henceforth assume that $|\mathbf{w}(0)| = |\mathbf{w}_0| = 1$ without loss of generality.

The initial/final frame orientation constraints are satisfied by choosing

$$\mathbf{w}_0 = \exp(i\frac{1}{2}\theta_0) \quad \text{and} \quad \mathbf{w}_2 = \gamma \exp(i\frac{1}{2}\theta_1)$$

where γ is a free (non-zero) real parameter. To match the prescribed end-point tangential angular velocities (10), we introduce the quantities

$$\rho_0 = \sigma(0) [\Omega_1(0) - \omega_1(0)] \quad \text{and} \quad \rho_1 = \sigma(1) [\Omega_1(1) - \omega_1(1)],$$

and one can then verify that the choice

$$\mathbf{w}_1 = \frac{\exp(i\frac{1}{2}\theta_1) \rho_0 + \exp(i\frac{1}{2}\theta_0) \gamma \rho_1}{4 \sin \frac{1}{2} \Delta\theta},$$

where $\Delta\theta = \theta_1 - \theta_0$, yields the desired initial/final values (10) of $\Omega_1(\xi)$.

The interpolants to the specified data (9) and (10) comprise a one-parameter family, dependent on the free variable γ . This variable can, in principle, be used to further optimize the frame variation² but it does not affect satisfaction of the boundary conditions. In the present study, to avoid further complicating the problem, we henceforth choose $\gamma = 1$ so that $|\mathbf{w}_2| = |\mathbf{w}_0|$.

Example 1. Consider the spatial PH quintic $\mathbf{r}(\xi)$ generated by the quadratic quaternion polynomial

$$\mathcal{A}(\xi) = \mathcal{A}_0 (1 - \xi)^2 + \mathcal{A}_1 2(1 - \xi)\xi + \mathcal{A}_2 \xi^2$$

with coefficients

$$\begin{aligned} \mathcal{A}_0 &= -0.951488 + 0.951488 \mathbf{i} + 0.394119 \mathbf{j} - 0.394119 \mathbf{k}, \\ \mathcal{A}_1 &= -0.208465 + 1.443549 \mathbf{i} - 0.298089 \mathbf{j} + 1.047198 \mathbf{k}, \\ \mathcal{A}_2 &= 1.229442 + 0.626432 \mathbf{i} + 1.376799 \mathbf{j} - 0.091481 \mathbf{k}. \end{aligned}$$

²The parameter γ was used in [10] to minimize the mean square deviation of the angular velocity component Ω_1 about the average value $\bar{\Omega}_1$.

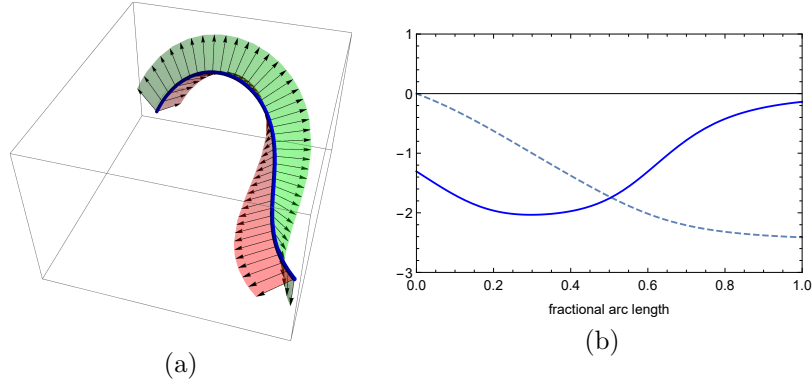


Figure 1: (a) ERF along the PH quintic in Example 1. The normal plane vectors $\mathbf{e}_2(\xi)$ and $\mathbf{e}_3(\xi)$ sweep out the green and red surfaces. (b) The angular velocity component $\omega_1(\xi)$ for the ERF is shown as the solid line, and the dashed line is its corresponding cumulative twist $T_{\text{ERF}}(\xi)$.

The ERF of this PH curve is shown in Figure 1(a), and the angular velocity ω_1 and the cumulative twist are plotted in Figure 1(b). The values of the angular velocity at the end points are $\omega_1(0) = -1.3052$ and $\omega_1(1) = -0.1374$; the total ERF twist is $T_{\text{ERF}} \approx -2.4115$.

We use this example to illustrate the dependence of the interpolant on the frame orientations at the end points. To clarify this dependence, we set all the boundary values except θ_1 to be zero, i.e.,

$$\theta_0 = 0, \quad \Omega_1(0) = 0, \quad \Omega_1(1) = 0.$$

Thus, the frames have the same orientation as the ERF at the start point, and exhibit no instantaneous rotation about the curve tangent at both end points. We compare solutions with the final angles $\theta_1 = \frac{1}{2}\pi$ and $\theta_1 = \pi$, as illustrated in Figures 2(a) and 2(b). The angular velocity component ω_1 and cumulative twist of these solution are shown in Figure 2(c)–(d). Comparing Figures 2(c) and 2(d), one can see that the values of the total twist differ by $\frac{1}{2}\pi$.

Example 2. We present a few more rational frame examples satisfying various Hermite data to illustrate the effect of the C^1 boundary conditions. The three rational frames in Figure 3 have the same end orientations

$$\theta_0 = 0 \quad \text{and} \quad \theta_1 = 2.4115 \approx -T_{\text{ERF}},$$

but different initial/final values of Ω_1 , namely

$$(a) \ \Omega_1(0) = -\Omega_1(1) = 1, \quad (b) \ \Omega_1(0) = \Omega_1(1) = 0, \quad (c) \ -\Omega_1(0) = \Omega_1(1) = 1.$$

The end orientations are fixed so that the initial frame agrees with the ERF, and the total twist is zero. Figures 3(a)–(c) show the resulting frame variations, while Figures 3(d)–(f) show the behavior of the angular velocity components Ω_1 as solid lines and the cumulative twist T as dashed lines.

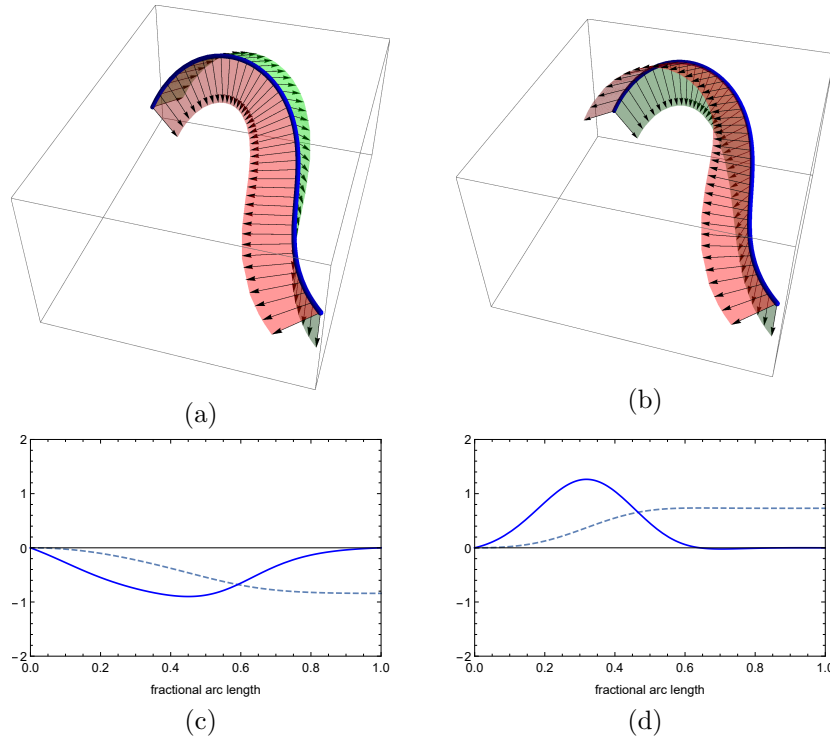


Figure 2: Rational adapted frames satisfying the Hermite boundary conditions $\theta_0 = 0$, $\Omega_1(0) = \Omega_1(1) = 0$ with end orientations (a) $\theta_1 = \frac{1}{2}\pi$ and (b) $\theta_1 = \pi$. Plots (c) and (d) illustrate the angular velocity component Ω_1 (solid line) and the cumulative twist T (dashed line) for the frames in (a) and (b), respectively.

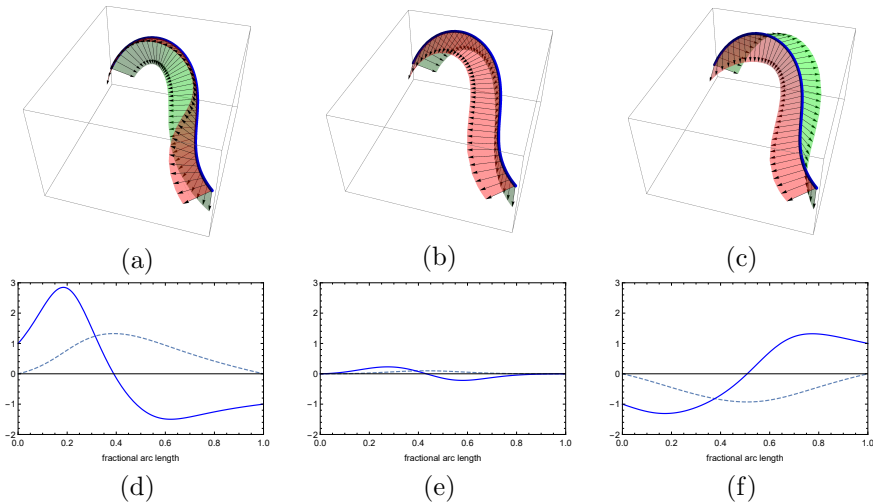


Figure 3: Comparison of rational frames with the same boundary orientations $\theta_0 = 0$ and $\theta_1 = -T_{\text{ERF}}$ but different boundary angular velocities — (a) $\Omega_1(0) = -\Omega_1(1) = 1$; (b) $\Omega_1(0) = \Omega_1(1) = 0$; (c) $-\Omega_1(0) = \Omega_1(1) = 1$. Figures (d)–(f) show graphs of the corresponding tangential angular velocity components Ω_1 (solid lines) and cumulative twists T (dashed lines).

4 Rational adapted spline frames

We now extend the end–point Hermite interpolation procedure, as described above, to the problem of constructing a piecewise–rational adapted frame along a spatial PH curve $\mathbf{r}(\xi)$ that interpolates given orientation data at a sequence of prescribed nodal parameter values with C^1 and C^2 continuity — i.e., continuity of the angular velocity (Section 4.3) and continuity of both the angular velocity and the angular acceleration (Section 4.4). We begin by introducing a method to represent the orientation data that eliminates ambiguities in its interpretation.

4.1 Representation of orientation data

Let $\xi_1, \dots, \xi_N \in (0, 1)$ with $\xi_0 = 0$ and $\xi_{N+1} = 1$ be nodal parameter values at which adapted frame orientations are to be specified. This data consists of orthonormal frame instances of the form

$$(\mathbf{f}_1(\xi_k), \mathbf{f}_2(\xi_k), \mathbf{f}_3(\xi_k)), \quad k = 0, \dots, N + 1$$

where it is understood that $\mathbf{f}_1(\xi_k)$ coincides with the curve tangent at $\mathbf{r}(\xi_k)$. The prescribed nodal frame orientations can be represented by phase angles θ_k relative to the ERF, such that

$$\begin{bmatrix} \mathbf{f}_2(\xi_k) \\ \mathbf{f}_3(\xi_k) \end{bmatrix} = \begin{bmatrix} \cos \theta_k & -\sin \theta_k \\ \sin \theta_k & \cos \theta_k \end{bmatrix} \begin{bmatrix} \mathbf{e}_2(\xi_k) \\ \mathbf{e}_3(\xi_k) \end{bmatrix}.$$

However, the angles θ_k must be considered indeterminate up to integer multiples of 2π , and this ambiguity can introduce undesired excess rotation of the normal-plane frame vectors.

We resolve this ambiguity as follows. At the initial point $\xi_0 = 0$, we use a prescribed phase angle $\theta_0 \in (-\pi, +\pi]$ and for each subsequent curve segment k we specify an incremental frame twist

$$\Delta T_k := T(\xi_k) - T(\xi_{k-1}) = \int_{\xi_{k-1}}^{\xi_k} \Omega_1(\xi) \sigma(\xi) d\xi, \quad k = 1, \dots, N + 1.$$

In view of the relation (7) between the tangential angular velocities of ERF and the frame $(\mathbf{f}_1(\xi), \mathbf{f}_2(\xi), \mathbf{f}_3(\xi))$, subsequent phase angles are nominally defined by

$$\theta_k = \theta_{k-1} + \Delta T_k - \Delta T_{\text{ERF},k} \quad (11)$$

where

$$\Delta T_{\text{ERF},k} := \int_{\xi_{k-1}}^{\xi_k} \omega_1(\xi) \sigma(\xi) d\xi$$

is the ERF twist along segment k . The cumulative ERF twist is defined by

$$T_{\text{ERF}}(\xi) := \int_0^\xi \omega_1(t) \sigma(t) dt, \quad (12)$$

and satisfies

$$T_{\text{ERF}}(\xi_k) = \sum_{i=1}^k \Delta T_{\text{ERF},i}. \quad (13)$$

Note that, for the spatial PH quintics, the integral (12) admits a closed-form reduction as described in [10].

Note that the formula (11) may produce θ_k values outside the range $(-\pi, \pi]$ and does not address the possibility that $|\Delta\theta_k| > 2\pi$. The desired frame is obtained by rotating the ERF using piecewise quadratic (or at most cubic) polynomials $\mathbf{w}(\xi) = a(\xi) + i b(\xi)$ and a single quadratic polynomial cannot incur a phase angle increment $> 2\pi$, since the winding angle of a parabola with respect to the origin cannot exceed 2π . Thus, if any segment $[\xi_{k-1}, \xi_k]$ has $|\Delta\theta_k| > 2\pi$, it should be subdivided by inserting an intermediate node.

To address these issues, we introduce the angular function

$$A(\xi) := \theta_0 + T(\xi) = \theta_0 + \int_0^\xi \Omega_1(t) \sigma(t) dt, \quad (14)$$

which equals the cumulative twist of the frame $(\mathbf{f}_1(\xi), \mathbf{f}_2(\xi), \mathbf{f}_3(\xi))$ plus the initial phase angle θ_0 . This function describes the phase angle relative to the RMF, starting from the initial orientation $(\mathbf{e}_1(0), \mathbf{e}_2(0), \mathbf{e}_3(0))$. If the orientation data for the frame $(\mathbf{f}_1(\xi), \mathbf{f}_2(\xi), \mathbf{f}_2(\xi))$ is specified by θ_0 and twist increments $\Delta T_k \in (-\pi, +\pi]$ for $k = 1, \dots, N + 1$ the corresponding values of $A(\xi_k)$ should be

$$A_k := A(\xi_k) = \theta_0 + \sum_{i=1}^k \Delta T_i. \quad (15)$$

k	ξ_k	ΔT_k	$\Delta T_{\text{ERF},k}$	θ_k	A_k
0	0.0			1.00000	1.0
1	0.1	0.5	-0.29533	1.79533	1.5
2	0.3	0.4	-0.63841	2.83374	1.9
3	0.6	-0.1	-0.87580	3.60954	1.8
4	0.8	-0.3	-0.40940	3.71894	1.5
5	1.0	0.0	-0.19257	3.91151	1.5

Table 1: Nodal orientation data generated from the specified initial orientation θ_0 and the sequence of incremental twist values ΔT_k in Example 3.

Thus interpolation of the given orientation data for the frame $(\mathbf{f}_1(\xi), \mathbf{f}_2(\xi), \mathbf{f}_3(\xi))$ can be interpreted as interpolation of the data (ξ_k, A_k) , $k = 0, \dots, N + 1$ by the function $A(\xi)$, and the phase angles are obtained from (13) and (15) as

$$\theta_k = A_k - T_{\text{ERF}}(\xi_k). \quad (16)$$

Example 3. Consider preparation of the orientation data for a new frame along the PH curve $\mathbf{r}(\xi)$ used in Example 1. The set of nodal parameters ξ_k is chosen as $\{0.0, 0.1, 0.3, 0.6, 0.8, 1.0\}$ and the initial phase angle is fixed as $\theta_0 = 1.0$, with incremental twist data specified by

$$\Delta T_1 = 0.5, \quad \Delta T_2 = 0.4, \quad \Delta T_3 = -0.1, \quad \Delta T_4 = -0.3, \quad \Delta T_5 = 0.0.$$

Converting these data into A_k and θ_k values as described above yields the results summarized in Table 1. Note that some of the θ_k values exceed π . These data are also illustrated graphically in Figure 4(a). The dashed line is the graph of the cumulative ERF twist (12), and the dots indicate the points (ξ_k, A_k) . The vertical lines indicate the phase angle values θ_k , as defined by (16).

The nodal frame orientations defined by the given data are illustrated in Figure 4(b) — the normal-plane vectors $\mathbf{f}_2(\xi_k)$ and $\mathbf{f}_3(\xi_k)$ are shown as green and red arrows, and small “fans” between them indicate the normal planes.

4.2 C^0 adapted spline frame

Based on the angular data representation described above, we begin by considering the simplest interpolant, namely, the C^0 rational spline frame. We construct a complex-valued piecewise-linear function $\mathbf{w}(\xi) = a(\xi) + i b(\xi)$ with segment $\mathbf{w}_k(\xi) = a_k(\xi) + i b_k(\xi)$ on $\xi \in [\xi_{k-1}, \xi_k]$ expressed in Bernstein form as

$$\mathbf{w}_k(\xi) = \frac{\mathbf{w}_{k,0}(\xi_k - \xi) + \mathbf{w}_{k,1}(\xi - \xi_{k-1})}{\Delta \xi_k},$$

with $\Delta \xi_k = \xi_k - \xi_{k-1}$. By choosing the values

$$\mathbf{w}_{k,0} = \exp(i \frac{1}{2} \theta_{k-1}) \quad \text{and} \quad \mathbf{w}_{k,1} = \gamma_k \exp(i \frac{1}{2} \theta_k)$$

with γ_k a free parameter, one can construct the C^0 spline frame by applying the rotation in Equation (5) to the ERF. This approach is very simple and

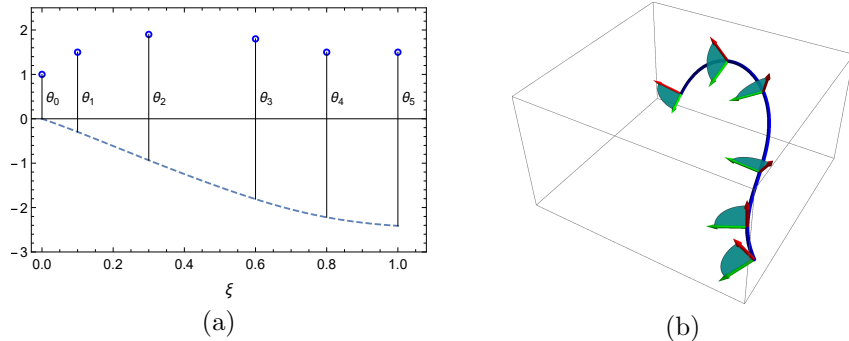


Figure 4: (a) The cumulative ERF twist $T_{\text{ERF}}(\xi)$ is plotted as the dashed line, and for each node ξ_k the A_k value is marked as a dot. The difference between A_k and $T_{\text{ERF}}(\xi_k)$ is equal to θ_k . (b) The orientation data are illustrated as pairs of vectors $\mathbf{f}_2(\xi_k)$ and $\mathbf{f}_3(\xi_k)$ indicated by green and red arrows.

straightforward. However, most practical applications require adapted frames with higher continuity than C^0 . In the following Sections, we consider spline frames with C^1 and C^2 continuity.

4.3 C^1 adapted spline frame

We here present a procedure to construct a C^1 rational adapted spline frame. For this purpose, we construct a complex-valued piecewise-quadratic function $\mathbf{w}(\xi) = a(\xi) + i b(\xi)$ with segment $\mathbf{w}_k(\xi) = a_k(\xi) + i b_k(\xi)$ expressed as

$$\mathbf{w}_k(\xi) = \frac{\mathbf{w}_{k,0}(\xi_k - \xi)^2 + \mathbf{w}_{k,1}2(\xi_k - \xi)(\xi - \xi_{k-1}) + \mathbf{w}_{k,2}(\xi - \xi_{k-1})^2}{(\Delta\xi_k)^2}.$$

By arguments analogous to those in Section 3, the values

$$\mathbf{w}_{k,0} = \exp\left(i\frac{1}{2}\theta_{k-1}\right) \quad \text{and} \quad \mathbf{w}_{k,2} = \gamma_k \exp\left(i\frac{1}{2}\theta_k\right) \quad (17)$$

with γ_k a free parameter, ensure matching of the orientation data θ_{k-1} and θ_k . As in Section 3, we henceforth choose $\gamma_k = 1$ for all k — this does not affect the nodal orientations or angular velocities, and ensures that $\mathbf{w}(\xi)$ is continuous. If the tangential component of the angular velocity at the node ξ_k is $\Omega_1(\xi_k)$, the coefficient $\mathbf{w}_{k,1}$ must be defined by

$$\mathbf{w}_{k,1} = \frac{\exp\left(i\frac{1}{2}\theta_k\right) \rho_{k-1} + \exp\left(i\frac{1}{2}\theta_{k-1}\right) \rho_k}{4 \sin \frac{1}{2}\Delta\theta_k} \Delta\xi_k \quad (18)$$

where $\Delta\theta_k = \theta_k - \theta_{k-1}$, and

$$\rho_k = \sigma(\xi_k) [\Omega_1(\xi_k) - \omega_1(\xi_k)]. \quad (19)$$

Now the nodal angular velocities $\Omega_1(\xi_k)$ are not specified *a priori*, but must be estimated from the given discrete orientation data. Recall that the function

(14) defines the phase angle of the frame $(\mathbf{f}_1(\xi), \mathbf{f}_2(\xi), \mathbf{f}_3(\xi))$ relative to the RMF, and interpolates the values A_k at the nodes ξ_k . Since $A'(\xi) = \Omega_1(\xi)\sigma(\xi)$, we can estimate $\Omega_1(\xi_k)$ as $A'(\xi_k)/\sigma(\xi_k)$. Hence, since $\sigma(\xi_k)$ is known, the problem is equivalent to estimating $A'(\xi_k)$ from the discrete data (ξ_k, A_k) . For sufficiently dense nodes, methods for numerical differentiation of unequally-spaced data [22] can furnish good estimates. However, we envisage that the method will also often be used with relatively sparse data, in which case a cubic spline that interpolates the points (ξ_k, A_k) offers good estimates for the $A'(\xi_k)$ values.

The nodal derivatives d_0, \dots, d_{N+1} of the C^2 cubic spline that interpolates the data points (ξ_k, A_k) for $k = 0, \dots, N+1$ are solutions [3] of the tridiagonal system of linear equations defined by

$$\begin{aligned} & \Delta\xi_{k+1} d_{k-1} + 2(\Delta\xi_k + \Delta\xi_{k+1}) d_k + \Delta\xi_k d_{k+1} \\ & = 3 \left[\Delta\xi_k \frac{A_{k+1} - A_k}{\Delta\xi_{k+1}} + \Delta\xi_{k+1} \frac{A_k - A_{k-1}}{\Delta\xi_k} \right] \end{aligned} \quad (20)$$

for $k = 1, \dots, N$ augmented by two *end conditions*. Two commonly used forms are quadratic end spans, in which case equations (20) are augmented by

$$d_0 + d_1 = 2 \frac{A_1 - A_0}{\Delta\xi_1} \quad \text{and} \quad d_N + d_{N+1} = 2 \frac{A_{N+1} - A_N}{\Delta\xi_{N+1}}, \quad (21)$$

and the “not-a-knot” end conditions, in which case we use

$$\begin{aligned} & (\Delta\xi_1 + \Delta\xi_2)\Delta\xi_2 d_0 + (\Delta\xi_1 + \Delta\xi_2)^2 d_1 \\ & = (3\Delta\xi_1 + 2\Delta\xi_2)\Delta\xi_2 \frac{A_1 - A_0}{\Delta\xi_1} + (\Delta\xi_1)^2 \frac{A_2 - A_1}{\Delta\xi_2}, \quad (22) \\ & (\Delta\xi_N + \Delta\xi_{N+1})^2 d_N + \Delta\xi_N(\Delta\xi_N + \Delta\xi_{N+1}) d_{N+1} \\ & = (\Delta\xi_{N+1})^2 \frac{A_N - A_{N-1}}{\Delta\xi_N} + \Delta\xi_N(2\Delta\xi_N + 3\Delta\xi_{N+1}) \frac{A_{N+1} - A_N}{\Delta\xi_{N+1}}. \end{aligned}$$

Note that both end conditions are consistent the tridiagonal nature of the linear system. Tridiagonal linear systems admit very simple and efficient solutions [3]. Once the solution has been obtained, we assign $A'(\xi_k) = d_k$ for $k = 0, \dots, N+1$. Finally the angular velocity estimate $\Omega_1(\xi_k)$ is obtained from

$$\Omega_1(\xi_k) = \frac{A'(\xi_k)}{\sigma(\xi_k)}, \quad (23)$$

which can be substituted into (19) to compute the middle coefficient (18).

Example 4. We apply the C^1 spline frame procedure to the data prepared in Example 3. After solving the linear system defined by (20) and the chosen end conditions, which is the quadratic end spans in this example, the nodal angular velocity values $\Omega_1(\xi_k)$ are obtained from (23), and the ρ_k values are computed from (19). These values are listed in Table 2. The next step is to construct the piecewise-quadratic function $\mathbf{w}(\xi) = a(\xi) + i b(\xi)$ with coefficients given by (17)

k	$\Omega_1(\xi_k)$	ρ_k
0	2.91468	8.95171
1	2.11576	6.91855
2	0.468119	3.90830
3	-0.911927	1.14273
4	-0.522730	0.453830
5	0.272692	1.56153

Table 2: Angular velocity estimates obtained from the cubic spline interpolant.

and (18), whose real and imaginary parts are used to construct a piecewise-rational frame by rotating the ERF through Equation (5). Figure 5(a) shows the resulting frame together with the given orientation data, while Figure 5(b) illustrates the variation of the phase angle $A(\xi)$ relative to the RMF (which interpolates the A_k data). Figure 5(c) shows the tangential angular velocity component $\Omega_1(\xi)$, which interpolates the data $\Omega_1(\xi_k)$. Since the frame has only C^1 continuity, the angular acceleration $\dot{\Omega}_1(\xi)$, shown in Figure 5(d), is discontinuous at the nodal points. Figure 5(e) shows plots of $a(\xi)$, $b(\xi)$, and $|\mathbf{w}(\xi)|$ as dashed blue, dotted red, and solid black lines, respectively.

4.4 C^2 adapted spline frame

The rational spline frame construction of the previous section yields only C^1 continuity — i.e., although the frame angular velocity is continuous, the angular acceleration is discontinuous at the nodal points (as seen in Figure 5(d)). Such acceleration discontinuities are impossible in the motion of physical bodies, since they require an infinite torque. Continuity of angular acceleration is equivalent to C^2 continuity of the frame, i.e., differentiability of the angular velocity $\boldsymbol{\Omega}$.

The angular velocity $\boldsymbol{\Omega}$ of the frame $(\mathbf{f}_1, \mathbf{f}_2, \mathbf{f}_3)$ has normal components that are identical to those of the angular velocity $\boldsymbol{\omega}$ of the ERF, and the tangential component Ω_1 differs only by the addition of the $\dot{\theta}$ term in (7). Since this term is defined by the expression (8), C^2 continuity of the functions $a(\xi)$, $b(\xi)$ implies C^2 continuity of Ω_1 . Hence, to achieve a C^2 frame, we seek to construct the functions $a(\xi)$ and $b(\xi)$ as C^2 cubic splines.

Note that C^2 continuity of $\mathbf{w}(\xi) = a(\xi) + i b(\xi)$ is a sufficient, though not necessary, condition for C^2 continuity of the frame. Since the phase angle $\theta(\xi)$ is defined in terms of $a(\xi)$ and $b(\xi)$ by (6), $\theta(\xi)$ may have higher continuity than $a(\xi)$ and $b(\xi)$ if these functions have nodal discontinuities that “cancel out” in the rational function $b(\xi)/a(\xi)$. In fact, this property was already used in the preceding section for construction of the C^1 rational spline frame. One may note in Figure 5(e) that the piecewise-quadratic functions $a(\xi)$ and $b(\xi)$ are not C^1 at the nodes, although the frame constructed from them is C^1 . One may, in principle, try to use this phenomenon to achieve higher frame continuity with a piecewise-quadratic function $\mathbf{w}(\xi)$, but this incurs complicated non-linear relations among the coefficients of adjacent quadratic segments. We adopt here

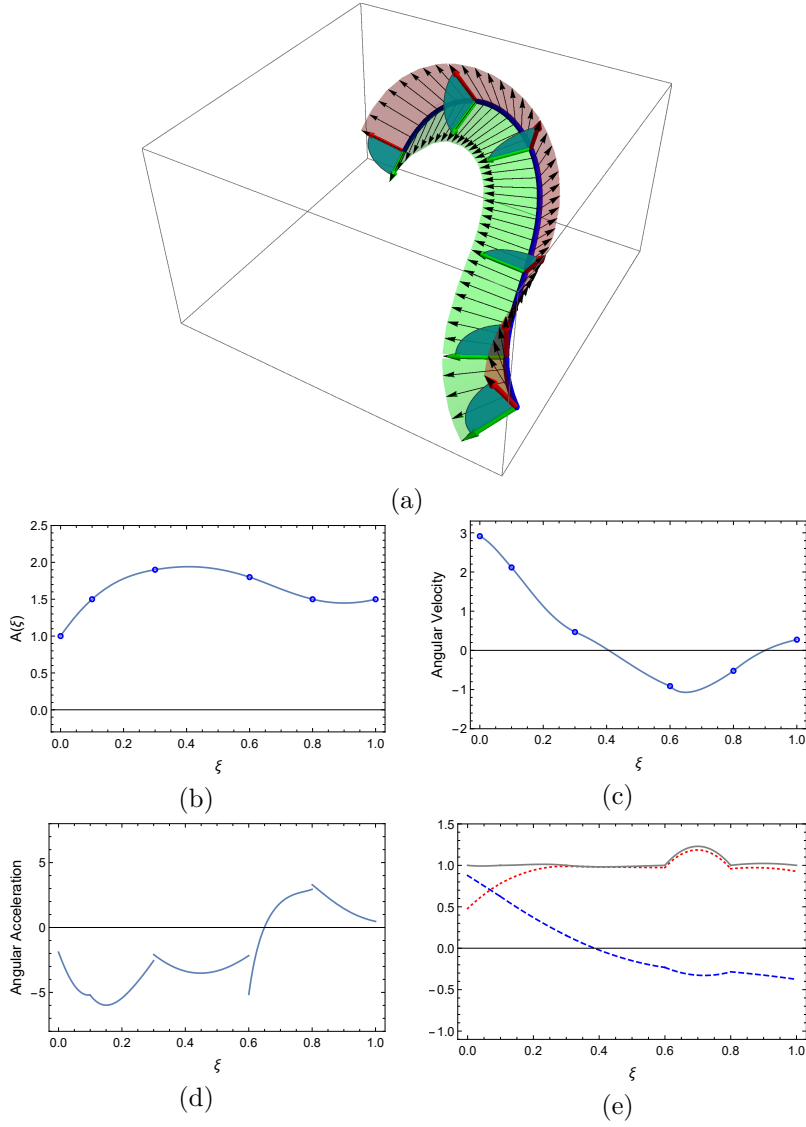


Figure 5: (a) The C^1 rational frame that interpolates the orientation data. (b) The phase angle function $A(\xi)$ with respect to the RMF. (c) The component $\Omega_1(\xi)$ of the frame angular velocity. (d) The tangential angular acceleration as the arc-length derivative of Ω_1 . (e) The piecewise-quadratic functions $a(\xi)$, $b(\xi)$ and the magnitude of the function $\mathbf{w}(\xi) = a(\xi) + ib(\xi)$ used to rotate the ERF are shown as dashed blue, dotted red, and solid black lines, respectively.

a simpler approach, based on the use of C^2 cubic splines.

Since the frame $(\mathbf{f}_1, \mathbf{f}_2, \mathbf{f}_3)$ is specified to have phase angles θ_k relative to the ERF at the nodes ξ_k , a C^2 rational adapted spline frame interpolating this data can be constructed from (5) by using C^2 piecewise-polynomial functions $a(\xi)$ and $b(\xi)$ that satisfy

$$\theta_k = 2 \tan^{-1} \frac{b(\xi_k)}{a(\xi_k)}, \quad k = 0, \dots, N + 1.$$

These conditions are fulfilled by real C^2 splines $a(\xi)$ and $b(\xi)$ that interpolate the points $\{\xi_k, \cos \frac{1}{2}\theta_k\}$ and $\{\xi_k, \sin \frac{1}{2}\theta_k\}$ — or, equivalently, by a C^2 complex spline $\mathbf{w}(\xi) = a(\xi) + i b(\xi)$ that interpolates $\{\xi_k, \exp(i\frac{1}{2}\theta_k)\}$. Setting $\mathbf{w}_k = \exp(i\frac{1}{2}\theta_k)$ and $\mathbf{d}_k = \mathbf{w}'(\xi_k)$, this cubic spline may be constructed by solving the tridiagonal system defined by (20) augmented by either of the end conditions (21) or (22), with $\mathbf{d}_0, \dots, \mathbf{d}_{N+1}$ and $\mathbf{w}_0, \dots, \mathbf{w}_{N+1}$ replacing d_0, \dots, d_{N+1} and A_0, \dots, A_{N+1} . Segment k of the resulting C^2 cubic spline is defined by

$$\mathbf{w}_k(u) := \mathbf{w}_{k-1}\alpha_0(u) + \mathbf{w}_k\alpha_1(u) + \Delta\xi_k [\mathbf{d}_{k-1}\beta_0(u) + \mathbf{d}_k\beta_1(u)],$$

where $u \in [0, 1]$ is the local variable on segment k defined by

$$u := \frac{\xi - \xi_{k-1}}{\Delta\xi_k},$$

and in terms of u the cubic Hermite basis functions are defined by

$$\begin{aligned} \alpha_0(u) &:= 1 - 3u^2 + 2u^3, & \alpha_1(u) &:= 3u^2 - 2u^3, \\ \beta_0(u) &:= u - 2u^2 + u^3, & \beta_1(u) &:= -u^2 + u^3. \end{aligned}$$

For PH quintics, the ERF vectors have a rational quartic dependence on the curve parameter. In the case of the C^1 spline, the rational rotation defined by (5) is quartic, so the normal-plane frame vectors $\mathbf{f}_2(\xi), \mathbf{f}_3(\xi)$ have a rational dependence of degree 8 on ξ . For the C^2 spline, the degree increases to 10.

Example 5. For the same PH curve as in Example 1 and the orientation data prepared in Example 3, we construct a C^2 adapted rational spline frame using the cubic spline $\mathbf{w}(\xi) = a(\xi) + i b(\xi)$ computed as described above. The resulting C^2 frame is shown in Figure 6(a), which on casual inspection appears similar to the C^1 frame in Figure 5(a). The difference is more apparent in the plot of the tangential angular velocity $\Omega_1(\xi)$ in Figure 6(c). The angular velocity data for the C^1 frame — i.e., the $\Omega_1(\xi_k)$ values in Example 5 — are indicated as dots in Figure 6(c), and small differences between the two frames can be seen. Moreover, the C^2 continuity of the new frame is evident in Figure 6(d) from the continuous graph of its tangential angular acceleration component. Figure 6(e) also shows that $a(\xi)$ and $b(\xi)$ have better behavior for the C^2 frame than for the C^1 frame, especially on the interval $[0.6, 0.8]$, and the magnitude of the cubic spline function $\mathbf{w}(\xi) = a(\xi) + i b(\xi)$ remains very close to 1.

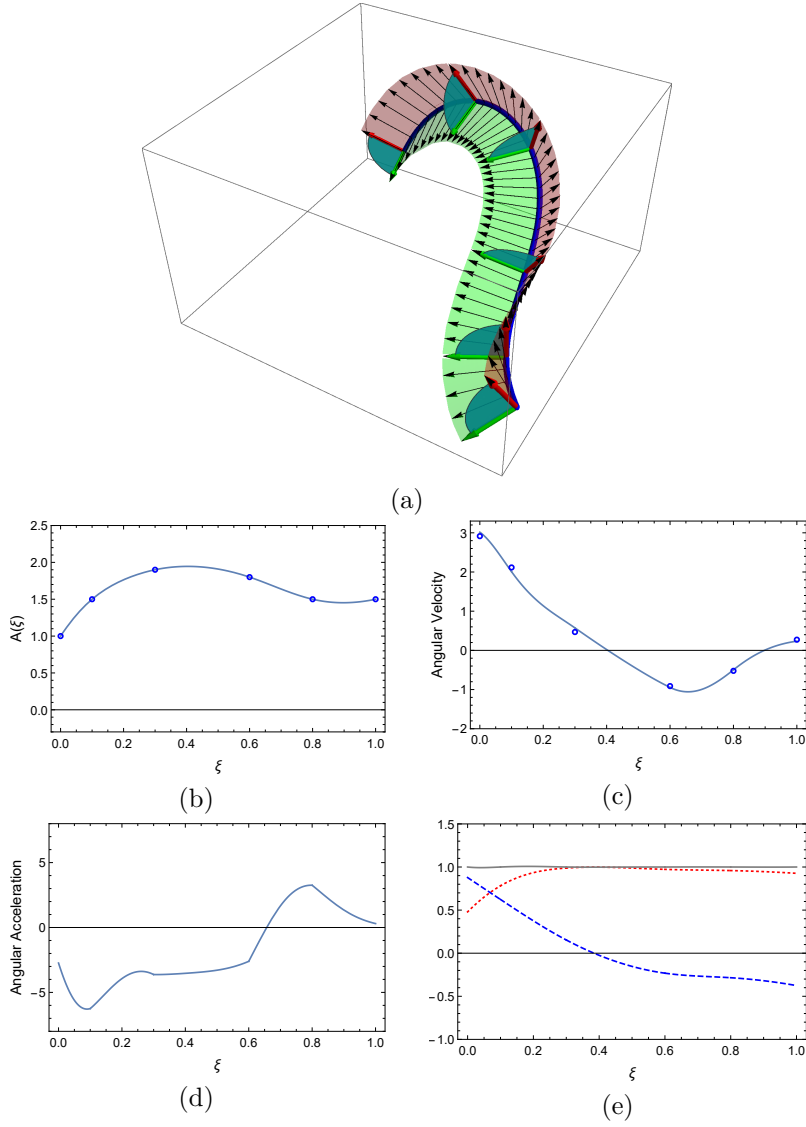


Figure 6: (a) The rational C^2 spline frame that interpolates the orientation data. (b) The phase angle function $A(\xi)$ with respect to the RMF. (c) The tangential component $\Omega_1(\xi)$ of the angular velocity. (d) The angular acceleration as the arc-length derivative of Ω_1 . (e) The piecewise-polynomial functions $a(\xi)$, $b(\xi)$ and the magnitude of the function $\mathbf{w}(\xi) = a(\xi) + i b(\xi)$ used to rotate the ERF are shown as dashed blue, dotted red, and solid black lines, respectively.

The method proposed in this article is applicable to various purposes. For example, one can use it to construct a rational approximation to the RMF, by setting all the frame twist increments T_k to zero in the orientation data. This is illustrated by the following Example.

Example 6. Consider the spatial quintic PH curve defined by

$$\begin{aligned}\mathcal{A}_0 &= -1.24029 + 1.24029 \mathbf{i} + 0.503913 \mathbf{j} + 0.907043 \mathbf{k}, \\ \mathcal{A}_1 &= -0.274494 + 0.692096 \mathbf{i} + 1.54218 \mathbf{j} - 1.12545 \mathbf{k}, \\ \mathcal{A}_2 &= 1.60629 + 0.818443 \mathbf{i} - 0.613094 \mathbf{j} + 0.934942 \mathbf{k}.\end{aligned}$$

Figure 7 (a) illustrates this curve together with its ERF. We choose evenly-spaced nodal parameters with step size 0.1. Then we fix the initial orientation as $\theta_0 = \frac{1}{2}\pi$, and set all the twist increments ΔT_k to zero. These orientation data agree with an RMF with an initial orientation of $\frac{1}{2}\pi$ relative to the ERF. The values of A_k , which is the phase angle from the RMF with the same initial position as the ERF, are then all equal to the same value $\frac{1}{2}\pi$, shown as dots in Figure 7 (b). The phase angle θ_k is the difference between A_k and the cumulative twist of the ERF, which is shown as dashed line in Figure 7 (b). The C^2 rational spline frame computed from these orientation data is shown in Figure 7 (c). Finally, Figure 7 (d) compares the angular velocities of the original ERF and the spline frame. Whereas the ERF angular velocity shows a strong variation, indicated by the dashed line, the angular velocity of the constructed spline frame (the solid line) is almost zero.

5 Closure

The problem of constructing a rational adapted spline frame interpolating given orientations at specified parameter values along a pre-defined spatial PH curve has been addressed. Such frames are generated by applying the rational rotation (5), constructed from a pair or real polynomials or a single complex polynomial, to the normal-plane vectors of the Euler-Rodrigues frame (ERF). When frame orientations and tangential angular velocities are specified at the curve end points, a Hermite interpolation problem can be solved using a complex quadratic polynomial through an extension of the approach developed in [10] to construct minimal twist frames. This methodology can be further generalized to construct C^1 rational adapted spline frames interpolating a given sequence of orientation data, using tangential angular velocity estimates based on the spline function that interpolates the frame phase angles relative to the ERF. To obtain a C^2 rational adapted spline frame, a method based on a complex cubic spline function $\mathbf{w}(\xi)$ that interpolates the complex exponentials of the phase angles is employed. This ensures continuity of angular acceleration at the nodal points, an important consideration in specifying physical rigid body motions.

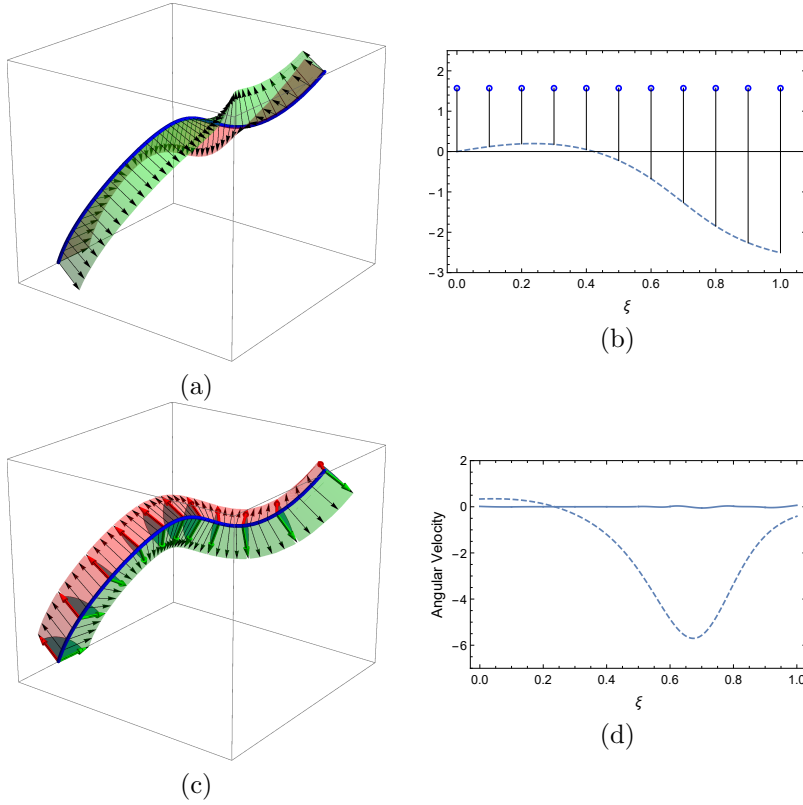


Figure 7: (a) The Euler-Rodrigues Frame of the spatial quintic PH curve. (b) The cumulative twist $T_{ERF}(\xi)$ of the ERF is plotted as the dashed line, and for each node ξ_k the phase angle values A_k is marked as a dot. (c) The rational C^2 spline frame that interpolates the given orientation data. (d) The angular velocity functions of the ERF and the spline frame are shown as dashed line and solid line, respectively.

Acknowledgment

The first author was supported by the research program of Dongguk University, 2017.

References

- [1] R.L. Bishop. There is more than one way to frame a curve. *American Mathematical Monthly*, 82:246–251, 1975.
- [2] H.I. Choi and C.Y. Han. Euler-Rodrigues frames on spatial Pythagorean-hodograph curves. *Computer Aided Geometric Design*, 19(8):603–620, 2002.
- [3] R.T. Farouki. *Pythagorean-Hodograph Curves: Algebra and Geometry Inseparable*. Springer, 2007.
- [4] R.T. Farouki. Quaternion and Hopf map characterizations for the existence of rational rotation-minimizing frames on quintic space curves. *Advances in Computational Mathematics*, 33:331–348, 2010.
- [5] R.T. Farouki. Rational rotation-minimizing frames—Recent advances and open problems. *Applied Mathematics and Computation*, 272:80–91, 2016.
- [6] R.T. Farouki, G. Gentili, C. Giannelli, A. Sestini, and C. Stoppato. A comprehensive characterization of the set of polynomial curves with rational rotation-minimizing frames. *Advances in Computational Mathematics*, 43:1–24, 2017.
- [7] R.T. Farouki, C. Giannelli, C. Manni, and A. Sestini. Design of rational rotation-minimizing rigid body motions by Hermite interpolation. *Mathematics of Computation*, 81:879–903, 2012.
- [8] R.T. Farouki and C.Y. Han. Rational approximation schemes for rotation-minimizing frames on Pythagorean-hodograph curves. *Computer Aided Geometric Design*, 20:435–454, 2003.
- [9] R.T. Farouki, C.Y. Han, P. Dospra, and T. Sakkalis. Rotation-minimizing Euler-Rodrigues rigid-body motion interpolants. *Computer Aided Geometric Design*, 30:653–671, 2013.
- [10] R.T. Farouki and H.P. Moon. Rational frames of minimal twist along space curves under specified boundary conditions. *Advances in Computational Mathematics*, 2018. <https://doi.org/10.1007/s10444-018-9599-3>.
- [11] R.T. Farouki and T. Sakkalis. Rational rotation-minimizing frames on polynomial space curves of arbitrary degree. *Journal of Symbolic Computation*, 45:844–856, 2010.

- [12] R.T. Farouki and T. Sakkalis. A complete classification of quintic space curves with rational rotation-minimizing frames. *Journal of Symbolic Computation*, 47:214–226, 2012.
- [13] C.Y. Han and S.-H. Kwon. Cubic helical splines with Frenet-frame continuity. *Computer Aided Geometric Design*, 28:395–406, 2011.
- [14] G. Jaklič, B. Jüttler, M. Krajnc, V. Vitrih, and E. Žagar. Hermite interpolation by rational G^k motions of low degree. *Journal of Computational and Applied Mathematics*, 240:20–30, 2013.
- [15] B. Jüttler. Generating rational frames of space curves via Hermite interpolation with Pythagorean hodograph cubic splines. In *Geometric Modeling and Processing '98*, pages 83–106. Bookplus Press, 1989.
- [16] B. Jüttler. Rotation minimizing spherical motions. In J. Lenarcic and M.L. Husty, editors, *Advances in Robot Kinematics: Analysis and Control*, pages 413–422. Springer, 1989.
- [17] B. Jüttler, M. Krajnc, and E. Žagar. Geometric interpolation by quartic rational spline motions. In J. Lenarcic and M. Stanisic, editors, *Advances in Robot Kinematics: Motion in Man and Machine*, pages 377–384. Springer, 2010.
- [18] B. Jüttler and C. Mäurer. Cubic Pythagorean hodograph spline curves and applications to sweep surface modelling. *Computer-Aided Design*, 31:73–83, 1999.
- [19] M. Krajnc and V. Vitrih. Motion design with Euler-Rodrigues frames of quintic Pythagorean-hodograph curves. *Mathematics and Computer in Simulation*, 82:1696–1711, 2012.
- [20] C. Mäurer and B. Jüttler. Rational approximation of rotation minimizing frames using Pythagorean hodograph cubics. *Journal for Geometry and Graphics*, 3:141–159, 1999.
- [21] K. Počkaj. Hermite G^1 rational spline motions of degree six. *Numerical Algorithms*, 66:721–739, 2014.
- [22] A.K. Singh and B.S. Bhadauria. Finite difference formulae for unequal sub-intervals using Lagrange’s interpolation formula. *International Journal of Mathematical Analysis*, 3(17):815–827, 2009.
- [23] Z. Sir and B. Jüttler. Spatial Pythagorean hodograph quintics and the approximation of pipe surfaces. In R. Martin, H. Bez, and M. Sabin, editors, *Mathematics of Surfaces XI*, pages 364–380. Springer, 2005.
- [24] W. Wang and B. Joe. Robust computations of the rotation minimizing frame for sweep surface modelling. *Computer-Aided Design*, 29:379–391, 1997.

- [25] W. Wang, B. Jüttler, D. Zheng, and Y. Liu. Computation of rotation minimizing frames. *ACM Transactions on Graphics*, 27:Article 2, 1–18, 2008.
- [26] Z. Zheng and G. Wang. Constructing rotation-minimizing frame of space Bézier curve. *Journal of Computer Aided Design & Computer Graphics*, 17:1785–1792, 2005.